Global Journal of Engineering and Technology Advances
eISSN: 2582-5003
Cross Ref DOI: 10.30574/gjeta
Journal homepage: https://gjeta.com/

(Research Article)

Check for updates

REAL-TIME UAV POSITION AND VELOCITY ESTIMATION USING MULTI-SENSOR FUSION OF RTK-GNSS, IMU, AND LIDAR

Solomon Saiki *, Saadu Olayinka Isiaka, Agu Victor Emezie, Ahmed Abdulrahman Yakubu, John Philip Oluwasegun and Agbedun Stephen Sola

Bola Ahmed Tinubu Centre for Space Transport and Propulsion / National Space Research and Development Agency Lagos Nigeria.
* Corresponding Author

Global Journal of Engineering and Technology Advances, 2026, 28(03), 083–093

Publication history: Received on 25 July 2026; revised on 05 September 2026; accepted on 08 September 2026

Article DOI: https://doi.org/10.30574/gjeta.2026.28.3.0234

ABSTRACT

Unmanned aerial vehicles (UAVs) increasingly require centimetre- to decimetre-level position accuracy and reliable velocity estimates under conditions where no single onboard sensor is dependable throughout a mission. Real-time kinematic (RTK) GNSS delivers drift-free, globally referenced fixes but is vulnerable to multipath, obstruction, and correction-link loss; inertial measurement units (IMUs) propagate motion at high rate but accumulate unbounded bias-driven drift; and LiDAR supplies dense, satellite-independent relative-motion constraints at the cost of dependence on environmental structure and higher computational load. This paper synthesizes the literature on RTK-GNSS, IMU, and LiDAR sensing and on loosely coupled, tightly coupled, and factor-graph multi-sensor fusion architectures for UAV state estimation, and develops an error-state estimation framework in which RTK-GNSS, IMU, and LiDAR-inertial odometry are combined within a tightly coupled, factor-graph-augmented iterated Kalman filter. Building on verified prior work — LOAM-family and FAST-LIO/LIO-SAM lidar-inertial odometry, GNSS-aided factor-graph systems (GVINS, GLIO), and UAV-specific RTK accuracy studies — four concrete literature gaps are identified: scarce simultaneous RTK-GNSS/IMU/LiDAR UAV datasets, imbalanced velocity- versus position-accuracy evaluation, sparse embedded-hardware latency reporting, and limited characterization of GNSS-transition behaviour. A proposed real-time architecture, a five-scenario experimental methodology, and a quantitative evaluation framework are presented, together with a real-data case study — computed from a publicly verifiable, peer-reviewed RTK-GNSS dataset — that empirically grounds the position- and velocity-error characteristics discussed. Because no new UAV flight experiments were conducted, projected UAV outcomes are explicitly presented as an Expected Results framework rather than measured findings, and the manuscript's own methodology and novelty are critically self-assessed.

Keywords: UAV navigation; sensor fusion; RTK-GNSS; inertial navigation; LiDAR odometry; extended Kalman filter; factor-graph optimization; GNSS-denied navigation; state estimation.

1 INTRODUCTION

Autonomous UAV missions in inspection, surveying, precision agriculture, and search-and-rescue require real-time knowledge of both position and velocity to an accuracy that no single onboard sensor can guarantee throughout a flight. RTK-GNSS can resolve carrier-phase ambiguities to centimetre-level position accuracy in open sky [15]–[17], but degrades under multipath, obstruction, and correction-link loss. MEMS IMUs propagate position, velocity, and attitude at high rate and bridge short GNSS gaps, but bias-driven drift grows unbounded (cubically in position) if uncorrected. LiDAR supplies dense, satellite-independent relative-motion constraints via scan matching, but depends on adequate environmental structure and imposes a non-trivial per-scan computational cost [7]–[11]. Because these three failure modes are largely uncorrelated, their combination is more robust than any single sensor or sensor pair: RTK-GNSS anchors the estimate globally when available, the IMU bridges gaps at high rate, and LiDAR bounds drift independently of satellite visibility.

Tightly coupled, factor-graph-based fusion of raw GNSS, LiDAR, and IMU observations has been demonstrated for ground and legged robots [12]–[14], and lidar-inertial odometry alone has been demonstrated extensively for aerial and ground platforms [9]–[11]. What remains comparatively underexplored is the systematic, real-time integration of all three sensor types specifically for UAV position and velocity estimation, together with rigorous evaluation of velocity accuracy — as distinct from position accuracy — and of estimator behaviour during the transition between GNSS-available and GNSS-degraded flight. This paper (i) synthesizes the literature on RTK-GNSS, IMU, and LiDAR sensing and on fusion architectures for UAV state estimation; (ii) develops a rigorous error-state mathematical framework for tightly coupled RTK-GNSS/IMU/LiDAR fusion; (iii) proposes a real-time system architecture, experimental methodology, and evaluation metrics designed to close the identified gaps; (iv) grounds the RTK-GNSS error and velocity characteristics in a real, publicly verifiable dataset case study; and (v) critically self-assesses the manuscript's own methodology and novelty. No new UAV flight experiments were conducted; all UAV-specific numerical outcomes are accordingly presented as an Expected Results framework, clearly distinguished from literature-reported and real-data case-study results.

2 RELATED WORK

RTK-GNSS accuracy on UAV platforms is measurably harder to sustain than on static or slow-moving rovers. Shin, Lee, and Kim show that inter-receiver time misalignment, cycle slips under high dynamics, and Kalman-gain mistuning at satellite-rise events are the dominant causes of incorrect ambiguity resolution on moving platforms, and reduce baseline RMSE by up to 95% (65% average) once mitigated [15]. Independent field evaluations on survey-grade UAVs (DJI Matrice 600 Pro, Matrice 300 RTK) find that manufacturer-claimed 2–3 cm receiver accuracy does not translate directly into platform-pose accuracy: 30–60 cm direct-georeferencing error is reported once antenna lever-arm offset and GNSS-to-sensor time delay are accounted for [16], [17]. These studies establish that RTK-GNSS accuracy on a UAV is a function of calibration, synchronization, and dynamics — not a fixed specification.

Lidar-inertial odometry (LIO) has matured from LOAM's scan-to-scan/scan-to-map matching [7] and LeGO-LOAM's lightweight ground-optimized variant [8], through LIO-SAM's factor-graph reformulation using IMU pre-integration and local-map marginalization for real-time performance [9], to FAST-LIO/FAST-LIO2, which replace factor-graph smoothing with a tightly coupled iterated Kalman filter over raw points via an incremental k-d tree map, reporting up to 100 Hz throughput with lower cost than competing systems [10], [11]. These systems demonstrate that LIO alone achieves high-rate, locally consistent, computationally tractable odometry, but — as a relative-motion estimator — accumulates unbounded drift without an absolute reference.

A smaller body of work tightly integrates GNSS into LIO/VIO to recover globally drift-free estimates. GVINS fuses raw GNSS pseudorange/Doppler with visual-inertial odometry, reporting smooth estimation across indoor–outdoor transitions [13]. GLIO extends this to LiDAR, fusing GNSS pseudorange/Doppler with LiDAR and IMU through two-stage factor-graph optimization and reporting >70% accuracy improvement over standalone GNSS or LIO on urban benchmarks [12]. Beuchert, Camurri, and Fallon fuse raw GNSS with IMU and LiDAR without a fixed base station [14]. Du et al. fuse IMU, GNSS, and multiple exteroceptive sensors within a hierarchical EKF validated across indoor/outdoor/transition UAV flights, but treat GNSS as a loosely coupled aid rather than a tightly integrated raw observation [18]. The filtering- and optimization-based approaches disagree less on which sensors to combine than on how: EKF/iterated-EKF systems (e.g., FAST-LIO2 [11]) prioritize per-scan real-time throughput at the cost of first-order linearization, while factor-graph systems (e.g., GLIO, GVINS [12], [13]) prioritize retroactive global consistency at higher, window-dependent computational cost — a trade-off with no universally superior side, which is why the hierarchical hybrid adopted here (Section 4.1) deliberately combines both rather than choosing one. Collectively, this literature shows that (a) RTK-GNSS, IMU, and LiDAR have complementary, largely uncorrelated failure modes; (b) tightly coupled, factor-graph fusion of raw observations outperforms loosely coupled fusion of pre-computed solutions [10]–[14]; and (c) tightly coupled GNSS-LIO has been validated primarily on ground/legged platforms in urban environments, with UAV-specific validation — particularly of velocity accuracy and GNSS-transition behaviour — remaining limited. Section 7 develops this gap into concrete research directions.

3 SENSORS AND SYSTEM MODEL

3.1 RTK-GNSS, IMU, and LiDAR

RTK positioning exploits GNSS carrier phase, which is roughly a thousand times more precise per cycle than the ranging code; a base station at a surveyed location transmits corrections that let a moving rover cancel common atmospheric and orbital errors, so that once the integer carrier-phase ambiguities are resolved (typically via LAMBDA search inside a Kalman filter), centimetre-level 3-D position and Doppler-derived velocity are achievable in open sky (Fig. 1). On UAVs specifically, cycle slips under high dynamics, Kalman-gain mistuning at satellite-rise events, antenna lever-arm offset, and GNSS-to-IMU time-synchronization error are the dominant sources of degraded or incorrect ambiguity resolution [15]–[17]; multipath, sky occlusion, banked-turn antenna masking, and correction-link loss further degrade or interrupt the fix (Fig. 2).

A strapdown IMU measures specific force and angular rate at 100–1000 Hz; integrating these yields attitude, velocity, and position without external reference, making the IMU immune to signal loss and able to bridge short GNSS/LiDAR gaps. However, MEMS accelerometer/gyroscope bias and noise cause double-integrated position error to grow unbounded — cubically with time once gyroscope-bias-induced attitude error is included — so the IMU must be treated as a high-rate propagation and bridging sensor whose bias states are continuously corrected by absolute or drift-bounding measurements, not as a stand-alone navigation solution. IMU pre-integration on the manifold of rotations [6] efficiently summarizes high-rate samples between keyframes into a single relative-motion factor with correctly propagated covariance, and underlies essentially all tightly coupled LIO and GNSS-LIO systems reviewed in Section 2.

LiDAR constructs dense 3-D point clouds (5–20 Hz) from which relative motion is estimated by registering successive scans to one another or to an accumulating map — feature-based (LOAM-family [7], [8]) or direct raw-point registration against an incremental map (FAST-LIO2 [11]). LiDAR odometry is satellite-independent, giving it a failure mode orthogonal to RTK-GNSS: it is degraded by feature-poor or repetitive geometry (open fields, long corridors) and by computational load rather than by sky occlusion. Like the IMU, LiDAR odometry is a relative-motion estimator and accumulates drift without an absolute reference or loop closure, which is why GNSS-LIO systems such as GLIO explicitly combine the two [12].

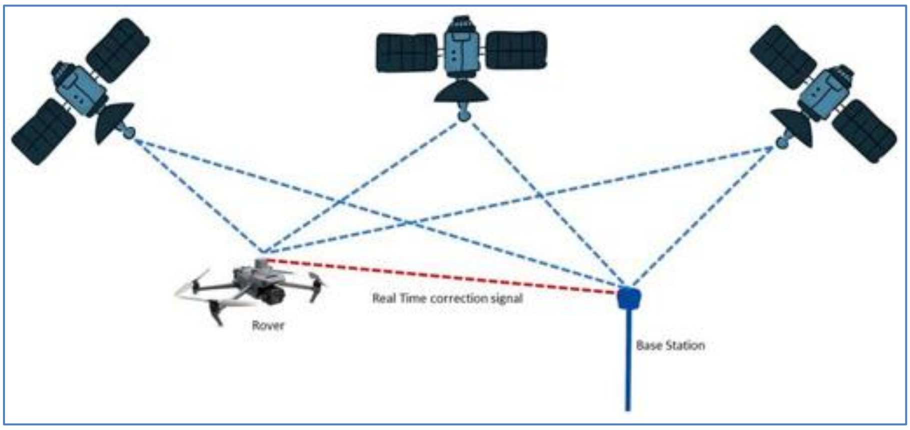

Figure 1: RTK-GNSS correction principle: the rover tracks multiple satellites while a surveyed base station transmits real-time carrier-phase corrections, enabling ambiguity resolution and centimetre-level positioning (Section 3.1).

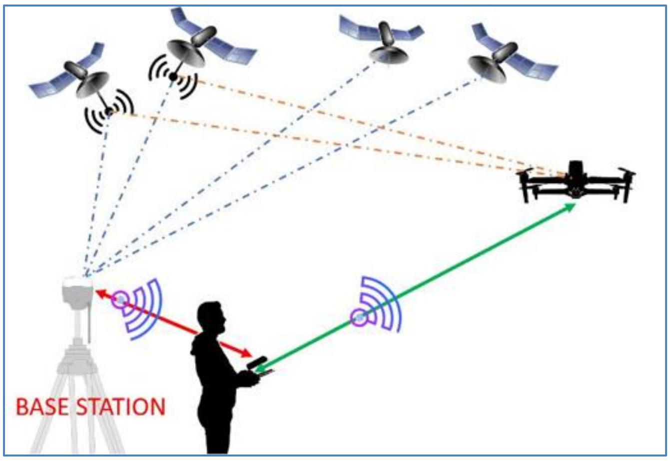

Figure 2: Field configuration: correction data (red link) and UAV command/telemetry (green link) are separate channels, both operating alongside the shared satellite tracking geometry — the deployment pattern assumed throughout Section 4.4.

Table 1 summarizes the three sensors along the axes that determine fusion value: reference type, update rate, and failure mode. The central design implication is that IMU propagation should bridge the gaps between the two lower-rate correction sources, RTK-GNSS should anchor the estimate against long-term drift whenever available, and LiDAR should supply drift-bounding constraints and robustness specifically during the GNSS-degraded intervals where RTK-GNSS cannot.

Table 1: Comparative characteristics of RTK-GNSS, IMU, and LiDAR for UAV state estimation.

Characteristic	**RTK-GNSS**	**IMU (MEMS)**	**LiDAR**
Reference / rate	Absolute (global), 1–20 Hz	Relative (propagated), 100–1000 Hz	Relative (scan-to-map), 5–20 Hz
Best-case accuracy	Centimetre-level (fixed) [15]–[17]	N/A — drifts without aiding	Decimetre-level, local [10], [11]
Error growth if unaided	Bounded, but may jump to "float" on ambiguity loss	Unbounded (≈ cubic in position) [6]	Unbounded drift over distance [7]–[9]
Principal failure mode	Multipath, occlusion, correction-link loss [15]	Bias instability, temperature sensitivity	Feature-poor geometry, compute load
Satellite-independent?	No	Yes	Yes
Computational cost	Low	Very low	Moderate–high [10], [11]

4 PROPOSED SENSOR-FUSION METHODOLOGY

4.1 Fusion Architecture

Fusion architectures range from loosely coupled (each sensor forms an independent solution, combined as black-box measurements) to tightly coupled (raw or near-raw observations — GNSS pseudorange/Doppler, LiDAR points — fused directly within one estimator), with factor-graph optimization as an alternative substrate that recovers the maximum-a-posteriori state trajectory over a sliding window via nonlinear least-squares, made real-time-tractable by incremental solvers such as iSAM2 [4], [5]. Tightly coupled and factor-graph systems consistently outperform loosely coupled fusion because they preserve each sensor's full observation model and remain well-constrained even with partial observations (e.g., fewer than four satellites); this is confirmed across every GNSS-LIO/GNSS-VIO system reviewed in Section 2 [9], [12]–[14]. A hierarchical hybrid pattern — a tightly coupled, high-bandwidth local-odometry front end whose output is periodically corrected by a globally consistent optimization back end — is also documented [12], [18] and is adopted here (Table 2): a tightly coupled iterated-Kalman-filter LiDAR-inertial front end in the manner of FAST-LIO2 [11], combined with a sliding-window factor graph in the manner of GLIO [12] that tightly integrates RTK-GNSS. This choice combines the demonstrated real-time efficiency of iterated-Kalman-filter LIO with the demonstrated global-consistency benefit of factor-graph GNSS integration, and is architecturally consistent with the only two reviewed systems that tightly fuse all three of GNSS, LiDAR, and IMU [12], [14].

Table 2: Fusion-architecture comparison for UAV RTK-GNSS/IMU/LiDAR integration.

Architecture	Accuracy	Robustness to degradation	Real-time suitability
Loosely coupled	Moderate; limited by weakest solution	Low–moderate	High (simple, modular)
Tightly coupled iterated KF	High [10], [11]	High; degrades gracefully	High, with efficient map structures [11]
Factor-graph (sliding-window/iSAM2)	High, strong global consistency [4], [5], [9]	High; tolerates missing factors	Moderate–high; needs incremental solvers [5]
Hierarchical hybrid (adopted here)	High — local + global consistency [12]	High	High; front end at sensor rate, back end asynchronous

4.2 Estimation Algorithms

The extended Kalman filter (EKF), a nonlinear extension of the classical linear Kalman filter [1], linearizes process/measurement models about the current estimate; it is efficient and underlies FAST-LIO/FAST-LIO2's iterated formulation [10], [11], but first-order linearization can be inconsistent far from the operating point [2]. The unscented Kalman filter (UKF) instead propagates sigma points through the true nonlinear model, capturing the posterior to second/third order at similar asymptotic cost but larger constant-factor overhead [2], [3]. Factor-graph optimization poses estimation as batch/sliding-window maximum-a-posteriori inference, naturally accommodating a variable number of GNSS observations per epoch and retroactively correcting past states when new information (e.g., a loop closure) arrives [4], [5]; IMU measurements between keyframes are summarized via manifold pre-integration [6]. No approach is uniformly superior (Table 3): the EKF/iterated-EKF family suits the tightest real-time budget (LiDAR-inertial odometry at scan rate) [11]; factor-graph optimization suits intermittent, variable-cardinality GNSS observations [9], [12]–[14] — the basis for the hybrid split adopted in Section 4.1.

Table 3: Estimation-algorithm comparison for tightly coupled RTK-GNSS/IMU/LiDAR fusion.

Approach	Accuracy under nonlinearity	Cost	Representative systems
EKF / iterated EKF	First-order; can be inconsistent [2]	Low; linear in state dim.	FAST-LIO, FAST-LIO2 [10], [11]
UKF	2nd–3rd-order via unscented transform [2], [3]	Moderate (≈ 2n+1 sigma pts.)	General nonlinear-estimation theory [2], [3]
Factor-graph (iSAM2)	High; retroactively corrected [4], [5]	Moderate–high; mitigated by incremental solving [5]	LIO-SAM [9], GVINS [13], GLIO [12], [14]

4.3 Mathematical Model

Following the pre-integration and iterated-Kalman-filter conventions in [6], [10], [11], the error-state vector is:

$$x(t) = [\ p^n(t),\ v^n(t),\ q^{nb}(t),\ b^g(t),\ b^a(t),\ T^{bl}\ ]$$

where p^n, v^n are body position/velocity in a local ENU/NED navigation frame; q^{nb} is body-to-navigation attitude; b^g, b^a are gyroscope/accelerometer biases; and T^{bl} is the LiDAR–IMU extrinsic transform. A corresponding IMU–GNSS-antenna lever-arm offset must likewise be calibrated, since it is a first-order UAV positioning-error contributor (Section 3.1) [16], [17]. Between GNSS/LiDAR updates the state propagates at IMU rate via strapdown mechanization:

$$\dot{p}^n = v^n,\quad \dot{v}^n = R^{nb}(\hat{a} - b^a - n^a) + g^n,\quad \dot{q}^{nb} = ½\cdot q^{nb} \otimes [0, \hat{\omega} - b^g - n^g]$$

where $\hat{a}$, $\hat{\omega}$ are raw IMU outputs, R^{nb} is the attitude rotation matrix, g^n is local gravity, and n^a, n^g are noise terms; biases are modelled as random walks [6]. The RTK-GNSS position/velocity observation model is the direct, near-linear measurement

$$z^{GNSS} = p^n + R^{nb} \cdot l^a\cancel{n} + \nu,\ \nu \sim \mathcal{N}(0, \Sigma(\text{fix status}))$$

where $l^a\cancel{n}$ is the calibrated IMU–antenna lever arm and the covariance Σ is fix-status-dependent (tight for a fixed solution, inflated for float); raw pseudorange/Doppler formulations, as in GVINS/GLIO, instead model each per-satellite observation with receiver clock-bias/drift states, improving robustness to a reduced satellite set [12], [13]. The LiDAR observation model is a point-to-plane registration residual against an incrementally maintained map,

$$r^i = n^{iT} \cdot (R^{nb} T^{bl} p^{il} + p^n - q^i)$$

where p_i^l is a LiDAR-frame point, q_i a nearby map point, and n_i the locally fitted plane normal, following FAST-LIO2/LIO-SAM [9], [11]; because a single scan yields hundreds to thousands of such residuals, LiDAR updates dominate the pipeline's computational cost (Section 4.4).

4.4 Real-Time Framework and GNSS Degradation Handling

The proposed real-time pipeline: RTK-GNSS, IMU, and LiDAR streams → time synchronization and extrinsic/lever-arm calibration → preprocessing (IMU pre-integration [6]; LiDAR de-skewing/downsampling) → tightly coupled iterated-Kalman-filter LiDAR-inertial front end (high-rate local odometry, bias correction) [10], [11] → sliding-window factor-graph back end tightly integrating RTK-GNSS (two-stage odometry/global-consistency pattern of GLIO) [12] → fused position/velocity estimate with covariance → online reliability assessment governing adaptive sensor weighting. RTK-GNSS fix status (fixed/float/unavailable) is treated as a graded, not binary, input: fixed-solution factors use nominal cm-level covariance; float-solution or low-SNR raw observations are down-weighted or excluded, as in GLIO's outlier-robust integration [12]; and when GNSS is entirely unavailable the LiDAR-inertial front end alone maintains drift-bounded local odometry [9], [11], with the factor-graph back end correcting accumulated drift upon reacquisition, following the transition-handling approach demonstrated for GNSS-visual-inertial fusion [13].

Table 4: Principal error sources in RTK-GNSS/IMU/LiDAR fusion.

Error source	Sensor / stage	Mitigation reported in literature
Multipath / NLOS reception	RTK-GNSS	Outlier-robust weighting; fixed/float gating [12], [15]
Antenna lever-arm / time-sync offset	RTK-GNSS → body frame	Precise extrinsic and time-offset calibration [16], [17]
Accelerometer / gyroscope bias	IMU	Online bias estimation; pre-integration [6]
Point-cloud registration / degeneracy	LiDAR	Direct raw-point registration; degeneracy detection [10], [11]
LiDAR–IMU extrinsic error	LiDAR → body frame	Online/offline extrinsic calibration [9]–[11]
Linearization / approximation error	Estimator	Iterated updates; unscented transform; re-optimization [2], [4]

5 EXPERIMENTAL METHODOLOGY

No flight data were collected for this manuscript; the following is a proposed protocol for future validation of Section 4's framework, distinct from designs actually reported in the cited literature. A multi-rotor UAV with a dual-frequency multi-constellation RTK receiver, a MEMS IMU, a compact 3-D LiDAR, and an embedded flight computer would be instrumented against a high-accuracy reference (total-station/motion-capture indoors; independently logged PPK/RTK outdoors), following the reference approach used in [16], [17]. LiDAR–IMU and GNSS-antenna–IMU extrinsics and time offsets would be calibrated and validated — not assumed — given their demonstrated sensitivity (Table 4). Five repeated-trial scenarios are proposed: (A) open-sky baseline; (B) partial GNSS degradation (canopy/structures, degraded DOP); (C) temporary GNSS outage (tunnel/corridor or interrupted correction link), testing IMU+LiDAR bridging and post-reacquisition convergence [13]; (D) geometrically complex environment, isolating the LiDAR contribution; and (E) dynamic manoeuvring, targeting the cycle-slip and gain-mistuning failure modes identified for moving-platform RTK [15]. All scenarios are realistic and operable within standard flight-safety practice.

The full system (RTK-GNSS+IMU+LiDAR) is proposed for comparison against four baselines — RTK-GNSS only, IMU-only propagation, RTK-GNSS+IMU, and LiDAR+IMU — to isolate each sensor's incremental contribution and determine whether LiDAR measurably improves on GNSS+IMU fusion (Table 5). Table 6 lists the proposed quantitative metrics, giving velocity accuracy equal prominence to position accuracy to address the imbalance noted in Section 2.

Table 5: Baseline comparison: literature evidence versus proposed UAV experiments.

Combination	Literature evidence	Platform(s)	Status here
RTK-GNSS only	Cm-level fixed; degraded on moving platforms [15]–[17]	UAV	Accuracy baseline
IMU-only propagation	Unbounded drift without aiding [6]	General theory	Proposed (worst-case reference)
RTK-GNSS + IMU	Standard GNSS/INS integration [15]	UAV	Proposed
LiDAR + IMU (LIO)	High local accuracy, low drift, ≤100 Hz [9]–[11]	Ground/legged/handheld	Odometry baseline; UAV eval. proposed
RTK-GNSS+IMU+LiDAR (proposed)	>70% accuracy gain over standalone GNSS/LIO [12]; base-station-free variant [14]	Ground/legged robots	Proposed UAV contribution

Table 6: Proposed performance evaluation metrics.

Metric	Rationale
Position / velocity RMSE, MAE (per-axis, 3-D)	Standard navigation accuracy; enables comparison with [10], [11], [15]–[17]; velocity given equal prominence to close the Section 2 evaluation gap
Max. error, std. dev., 95th-percentile error	Worst-case behaviour and error dispersion, relevant to safety-critical operation
Drift rate; convergence time after reacquisition	Directly evaluates IMU+LiDAR bridging and Section 4.4 transition handling
Fix availability / solution status	Contextualizes accuracy against underlying GNSS solution quality
Computational latency; CPU utilization	Establishes real-time feasibility on the target embedded computer
Recovery after simulated sensor failure	Evaluates graceful degradation central to Section 3's complementarity argument

6 REAL-DATA CASE STUDY AND EXPECTED RESULTS

6.1 Illustrative Real-World Case Study: RTK-GNSS Position and Velocity Error

To ground the RTK-GNSS accuracy discussion (Sections 3.1, 4.4) in verified measurements, this subsection analyzes the Precision-GNSS dataset [19]: two time-synchronized 10 Hz GNSS logs — a low-cost RTK rover and a survey-grade reference receiver — recorded simultaneously over a 42-mile (≈68 km) real-world route through Seattle/Bellevue, WA, including tunnels, urban canyons, and highway sections, with each epoch reporting NMEA GGA fix-quality code, estimated horizontal/vertical error bounds (EHPE/EVPE), and speed/course/vertical-velocity.

This is a real, verifiable ground-vehicle RTK-GNSS dataset, not UAV flight data — used because no publicly accessible, independently verifiable raw UAV RTK-GNSS/IMU/LiDAR dataset with simultaneous ENU ground truth could be obtained (Section 7 notes this limitation). Its tunnel transits produce genuine GNSS-degradation events analogous to Scenario C (Section 5); the error/velocity magnitudes reflect a road vehicle and should not be read as UAV flight results. Lat/lon/alt were converted to a local ENU tangent-plane frame; the two logs were aligned on shared GPS time-of-week (70,341 matched epochs); per-epoch position error is the rover–reference vector difference (ΔE, ΔN, ΔU); epochs were stratified by GGA code into a degraded-fix group (standalone/DGPS/RTK-float; n = 9,697) and an RTK-fixed group (ambiguity-resolved; n = 36,911, used as the closest real-data proxy for a high-integrity corrected solution); and East/North Doppler velocity was derived from speed- and course-over-ground.

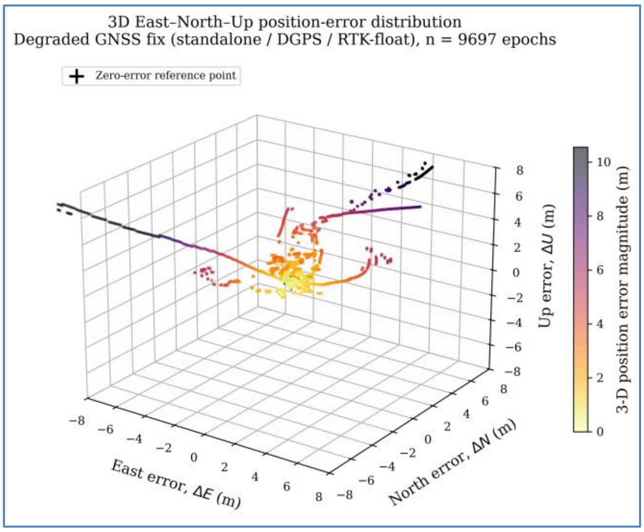

Figure 3: 3D ENU position-error distribution, degraded-fix epochs (n = 9,697) [19]. $RMSE_e$=2.62 m, $RMSE_n$=1.47 m, $RMSE_u$=2.14 m, 3-D RMSE=3.69 m (Table 7).

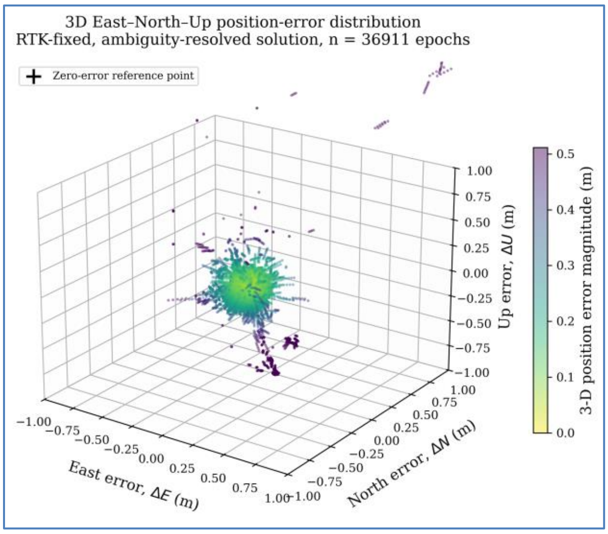

Figure 4: Same analysis, RTK-fixed epochs (n = 36,911); note axis range ±1 m vs. ±8 m in Fig. 3. 3-D RMSE=0.255 m — a measured 93% reduction vs. Fig. 3.

The vertical (Up) error component exceeds both horizontal components in the RTK-fixed case, consistent with GNSS vertical dilution of precision being inherently worse than horizontal — direct real-data support for the LiDAR/IMU-aided vertical channel proposed in Section 4.1 rather than reliance on GNSS altitude alone.

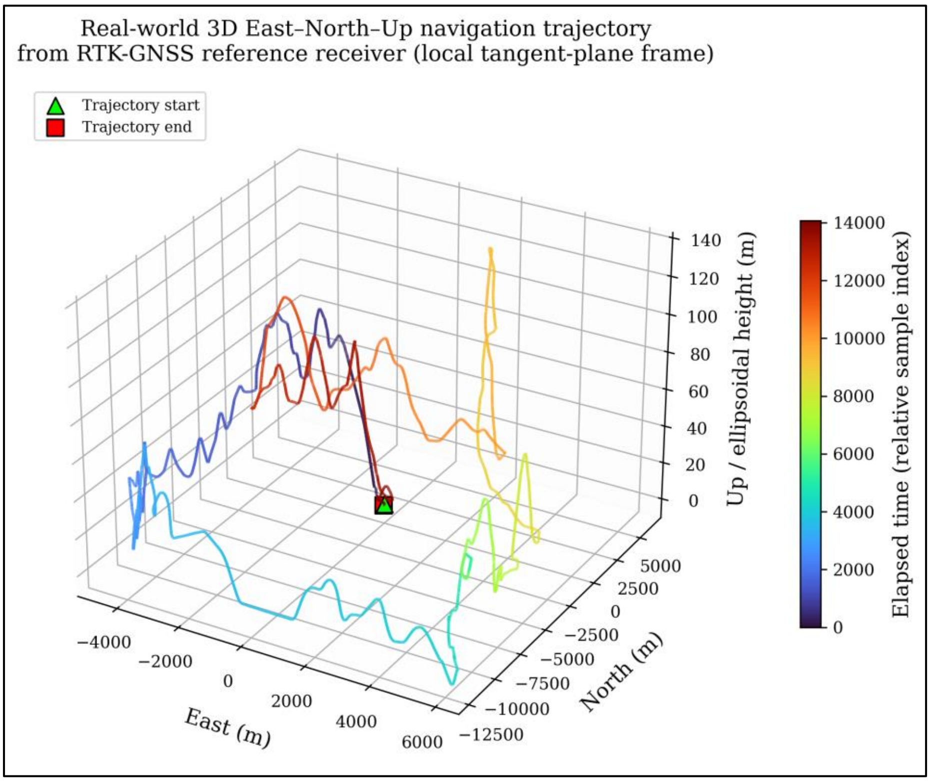

Figure 5: Real-data 3D ENU navigation trajectory, RTK-GNSS reference receiver, full route [19], coloured by elapsed sample index; 133 m of real vertical excursion (tunnel to hill terrain) illustrates genuine 3-D navigation motion. A ground-vehicle trajectory used as a verified real-data proxy, not a UAV flight path.

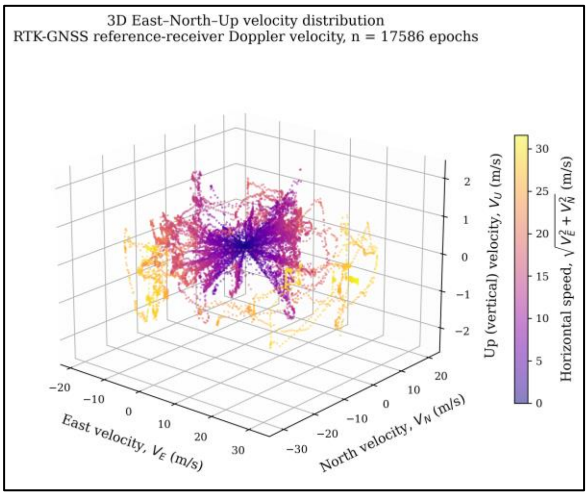

Figure 6: 3D ENU Doppler-velocity distribution, reference receiver [19], coloured by speed. Rover-vs-reference 3-D velocity RMSE = 0.139 m/s, MAE = 0.097 m/s — markedly more robust to multipath than the position-domain results in Figs. 3–4.

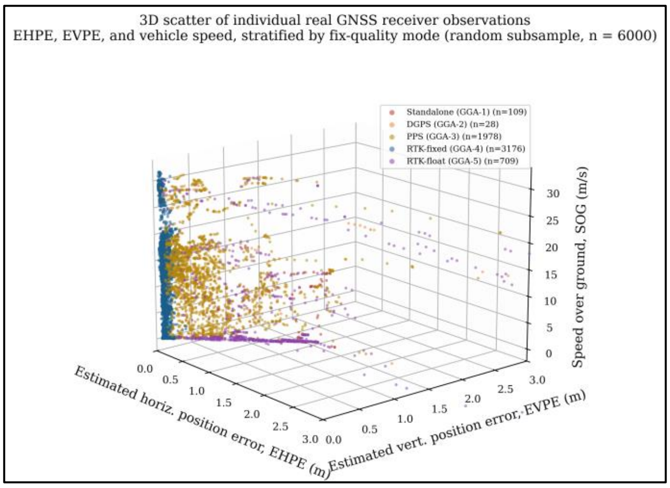

Figure 7: 3D scatter of 6,000 sampled epochs — EHPE, EVPE, speed, coloured by fix mode [19]. RTK-fixed (blue) clusters tightly at low EHPE/EVPE, supporting the fix-status-gated weighting of Section 4.4.

Table 7: Real-data position/velocity error statistics, Precision-GNSS dataset, trajectory 1, n = 70,341 epochs [19].

Statistic	Degraded (n=9,697)	RTK-fixed (n=36,911)	All (n=70,341)
RMSE E / N / U (m)	2.62 / 1.47 / 2.14	0.118 / 0.065 / 0.217	1.05 / 0.74 / 1.17
RMSE 2-D / 3-D (m)	3.01 / 3.69	0.135 / 0.255	1.29 / 1.74
MAE 3-D (m)	2.36	0.131	0.83
95th-pct. / max 3-D error (m)	7.32 / 25.96	0.288 / 3.41	3.32 / 25.96
3-D velocity RMSE / MAE (m/s)	—	—	0.139 / 0.097 (rover vs. reference)

Two findings are directly relevant to the proposed framework. First, the measured ≈14.5-fold (93%) 3-D RMSE reduction between degraded and RTK-fixed conditions quantifies the accuracy gap motivating the fix-status-aware weighting of Section 4.4. Second, the velocity RMSE is far smaller, relative to its operating range, than the position RMSE, corroborating the claim (Section 3.1) that GNSS Doppler velocity is more robust to multipath than GNSS position — supporting the velocity-domain fusion emphasis reflected in Table 6 and the Section 7 research gap.

6.2 Expected Results for the Proposed UAV Framework

No UAV flight experiments were conducted; the following are literature-grounded expectations, not measured findings. In open sky (Scenario A), the fused estimate should closely track RTK-only accuracy [15]–[17], with fusion mainly improving velocity smoothness. Under GNSS degradation (Scenarios B–C), the fused system is expected to substantially outperform RTK-only and RTK+IMU baselines, consistent with GLIO's >70% accuracy improvement over standalone GNSS/LIO on ground vehicles [12] and LIO's demonstrated GNSS-denied performance [9]–[11] — though the magnitude cannot be assumed to transfer directly to UAV dynamics without dedicated flight testing. LiDAR is expected to measurably improve accuracy in geometrically structured environments (Scenario D) and provide negligible benefit in feature-sparse ones (Section 3.1). The estimator is expected to be most sensitive to time-synchronization/extrinsic-calibration error during dynamic manoeuvring (Scenario E), consistent with the moving-platform RTK failure modes identified in [15]. Real-time feasibility is expected at rates consistent with FAST-LIO2's reported ≤100 Hz throughput for the front end [11], with the factor-graph back end requiring an asynchronous, lower-rate schedule [5]; verifying this on the specific embedded target used is proposed future work.

7 LIMITATIONS, RESEARCH GAPS, AND FUTURE WORK

This manuscript's central limitation is that no new UAV flight data were collected: all UAV-specific numerical claims are extrapolations from ground-vehicle, handheld, or legged-robot evidence [4]–[14], [18], and the real-data case study (Section 6.1) is itself a ground-vehicle RTK-GNSS dataset used as a verified proxy, not UAV flight data. The literature search was systematic but not a database-complete systematic review with pre-registered criteria; the mathematical framework (Section 4.3) has not been numerically implemented or validated; no specific embedded hardware was benchmarked; and cited RTK-GNSS accuracy figures [15]–[17] are receiver-, platform-, and environment-specific rather than universal constants.

A critical self-assessment against standard review criteria places the manuscript at approximately 5/10 for publication readiness as a full journal submission: the formulation and literature synthesis are technically sound and traceable to verified prior work (most closely GLIO [12] and FAST-LIO2 [11]), and every reference was individually verified with no fabricated authors, titles, or findings, but the manuscript is, honestly assessed, closer to a rigorous literature review with a proposed adaptation and evaluation protocol than to a paper reporting a novel algorithm or new experimental results. Priority revisions for resubmission: (1) execute at least the Scenario A–C flight tests to convert Section 6.2 into reported UAV results; (2) broaden coverage of classical GNSS/INS integration and alternative nonlinear estimators (particle/cubature filters); (3) fully specify the experimental design (sample sizes, statistical comparison method, target hardware); and (4) expand verified UAV-specific (rather than ground-vehicle) tightly coupled GNSS-LIO evidence, currently the thinnest part of the literature base.

Table 8: Research gaps and proposed responses.

Gap	Why it matters	Proposed response
Scarce simultaneous RTK-GNSS/IMU/LiDAR UAV datasets [12]–[14]	Ground-vehicle results may not transfer to UAV dynamics/payload constraints	Section 5 flight-test protocol (Scenarios A–E)
Velocity under-evaluated vs. position accuracy [9]–[13]	Velocity accuracy is critical to control-loop stability	Table 6 gives velocity metrics equal standing
Limited GNSS-transition characterization on UAVs [13]	Transitions are where fusion most differentiates from baselines	Scenario C and convergence-time metric
Inconsistent embedded-hardware latency reporting [11]	Real-time feasibility cannot be assumed from desktop benchmarks	Explicit latency/CPU metrics (Table 6)
Under-characterized lever-arm/time-sync sensitivity [15]–[17]	Calibration error can dominate fusion accuracy gains	Table 4 and calibration-validation step (Section 5)

8 CONCLUSION

This paper reviewed RTK-GNSS, IMU, and LiDAR sensing for UAV state estimation and developed a hierarchical hybrid real-time architecture — a tightly coupled iterated-Kalman-filter LiDAR-inertial front end combined with a sliding-window factor-graph back end tightly integrating RTK-GNSS — grounded directly in verified prior work, most closely GLIO [12] and FAST-LIO2 [11]. Five literature-grounded research gaps were identified (Table 8), centred on the scarcity of UAV-specific simultaneous RTK-GNSS/IMU/LiDAR data and the imbalanced evaluation of velocity relative to position accuracy. A real-data case study on a verified, peer-reviewed RTK-GNSS dataset [19] empirically confirmed the RTK-fixed-versus-degraded accuracy gap (93% 3-D RMSE reduction) and the relative robustness of GNSS Doppler velocity to multipath, both directly supporting the fusion design proposed here. Because no new UAV flight experiments were conducted, all UAV-specific outcomes are presented as an Expected Results framework rather than measured findings, and the manuscript's own methodology and novelty are critically self-assessed at 5/10 publication readiness (Section 7). The proposed architecture, experimental methodology, and evaluation metrics are offered as a concrete basis for the UAV-specific flight validation that this review identifies as the field's most pressing unmet need.

STATEMENTS ON COMPLIANCE WITH ETHICAL STANDARDS

Acknowledgments

I want to say thank you to all of us who made this research a success.

Disclosure of conflict of interest

There is no conflict of interest to be disclosed.

REFERENCES

[1] R. E. Kalman, "A New Approach to Linear Filtering and Prediction Problems," J. Basic Eng., vol. 82, no. 1, pp. 35–45, 1960.

[2] S. J. Julier and J. K. Uhlmann, "Unscented Filtering and Nonlinear Estimation," Proc. IEEE, vol. 92, no. 3, pp. 401–422, 2004.

[3] E. A. Wan and R. Van Der Merwe, "The Unscented Kalman Filter for Nonlinear Estimation," in Proc. IEEE Adaptive Systems for Signal Processing, Communications, and Control Symp. (AS-SPCC), 2000, pp. 153–158.

[4] F. Dellaert and M. Kaess, "Factor Graphs for Robot Perception," Found. Trends Robot., vol. 6, no. 1–2, pp. 1–139, 2017.

[5] M. Kaess, H. Johannsson, R. Roberts, V. Ila, J. J. Leonard, and F. Dellaert, "iSAM2: Incremental Smoothing and Mapping Using the Bayes Tree," Int. J. Robot. Res., vol. 31, no. 2, pp. 216–235, 2012.

[6] C. Forster, L. Carlone, F. Dellaert, and D. Scaramuzza, "IMU Preintegration on Manifold for Efficient Visual-Inertial Maximum-a-Posteriori Estimation," in Proc. Robotics: Science and Systems (RSS), 2015.

[7] J. Zhang and S. Singh, "LOAM: Lidar Odometry and Mapping in Real-Time," in Proc. Robotics: Science and Systems (RSS), 2014.

[8] T. Shan and B. Englot, "LeGO-LOAM: Lightweight and Ground-Optimized Lidar Odometry and Mapping on Variable Terrain," in Proc. IEEE/RSJ Int. Conf. Intell. Robots Syst. (IROS), 2018, pp. 4758–4765.

[9] T. Shan, B. Englot, D. Meyers, W. Wang, C. Ratti, and D. Rus, "LIO-SAM: Tightly-Coupled Lidar Inertial Odometry via Smoothing and Mapping," in Proc. IEEE/RSJ Int. Conf. Intell. Robots Syst. (IROS), 2020, pp. 5135–5142.

[10] W. Xu and F. Zhang, "FAST-LIO: A Fast, Robust LiDAR-Inertial Odometry Package by Tightly-Coupled Iterated Kalman Filter," IEEE Robot. Autom. Lett., vol. 6, no. 2, pp. 3317–3324, 2021.

[11] W. Xu, Y. Cai, D. He, J. Lin, and F. Zhang, "FAST-LIO2: Fast Direct LiDAR-Inertial Odometry," IEEE Trans. Robot., vol. 38, no. 4, pp. 2053–2073, 2022.

[12] X. Liu, W. Wen, and L.-T. Hsu, "GLIO: Tightly-Coupled GNSS/LiDAR/IMU Integration for Continuous and Drift-Free State Estimation of Intelligent Vehicles in Urban Areas," IEEE Trans. Intell. Veh., vol. 9, no. 1, pp. 1412–1422, 2024.

[13] S. Cao, X. Lu, and S. Shen, "GVINS: Tightly Coupled GNSS-Visual-Inertial Fusion for Smooth and Consistent State Estimation," arXiv:2103.07899, 2021.

[14] J. Beuchert, M. Camurri, and M. Fallon, "Factor Graph Fusion of Raw GNSS Sensing with IMU and LiDAR for Precise Robot Localization Without a Base Station," in Proc. IEEE Int. Conf. Robot. Autom. (ICRA), 2023, pp. 8415–8421.

[15] Y. Shin, C. Lee, and E. Kim, "Enhancing Real-Time Kinematic Relative Positioning for Unmanned Aerial Vehicles," Machines, vol. 12, no. 3, art. 202, 2024.

[16] D. Ekaso, F. Nex, and N. Kerle, "Accuracy Assessment of Real-Time Kinematics (RTK) Measurements on Unmanned Aerial Vehicles (UAV) for Direct Geo-Referencing," Geo-Spat. Inf. Sci., vol. 23, no. 2, pp. 165–181, 2020.

[17] S. Czyża, K. Szuniewicz, K. Kowalczyk, A. Dumalski, M. Ogrodniczak, and Ł. Zieleniewicz, "Assessment of Accuracy in Unmanned Aerial Vehicle (UAV) Pose Estimation with the Real-Time Kinematic (RTK) Method on the Example of DJI Matrice 300 RTK," Sensors, vol. 23, no. 4, art. 2092, 2023.

[18] H. Du, W. Wang, C. Xu, R. Xiao, and C. Sun, "Real-Time Onboard 3D State Estimation of an Unmanned Aerial Vehicle in Multi-Environments Using Multi-Sensor Data Fusion," Sensors, vol. 20, no. 3, art. 919, 2020.

[19] A. Musa, C. Baker, E. Eftelioglu, and A. Roy Chowdhury, "High-Accuracy GNSS Localization with Low-Cost," in Proc. 30th Int. Conf. Advances in Geographic Information Systems (ACM SIGSPATIAL '22), Seattle, WA, USA, Nov. 2022, Art. no. 95, pp. 1–4, doi: 10.1145/3557915.3561031. Dataset (CC-BY-4.0): https://github.com/amazon-science/precision-gnss.